

# Jordan Journal of Physics

## ARTICLE

---

### Structural and Magnetic Properties of $\text{Pr}_{0.7}\text{Bi}_{0.3}\text{Mn}_{1-x}\text{Fe}_x\text{O}_3$ ( $0 \leq x \leq 0.2$ ) Manganites Oxides Prepared by Sol-gel Method

Kh. Sbissi<sup>a</sup>, D. Fatnassi<sup>a</sup>, M. Ellouze<sup>b</sup>, E. K. Hlil<sup>c</sup> and F. Elhalouani<sup>a</sup>

<sup>a</sup> University of Sfax, National Engineering School of Sfax, B. P. W-3038, Tunisia.

<sup>b</sup> University of Sfax, Faculty of Sciences of Sfax, B. P. 1171, 3000, Tunisia.

<sup>c</sup> Institut Néel, B. P. 166, B. P. W-38042 Grenoble Cedex 9, France.

---

Received on: 5/1/2015; Accepted on: 8/3/2015

---

**Abstract:** The morphology, structural and magnetic properties of  $\text{Pr}_{0.7}\text{Bi}_{0.3}\text{Mn}_{1-x}\text{Fe}_x\text{O}_3$  manganites oxides, prepared by sol-gel method, have been investigated to study the effect of the substitution of Mn by Fe. X-ray powder diffraction, Scanning Electron Microscopy (SEM), Fourier transforms infrared spectroscopy (FT-IR) and magnetic measurements for the systems have been investigated. Rietveld analysis of the X-ray powder diffraction show that the samples crystallize in the orthorhombic perovskite system with Pnma space group. The average particle size of about 60 nm was obtained from X-ray diffraction. We have found that with increasing x doping concentration of Fe, the unit cell volume decreases. Magnetic measurements *versus* temperature with an applied magnetic field of 0.05T show that all samples exhibit antiferromagnetic to paramagnetic transition with increasing temperature, at Neel temperature.

**Keywords:** Sol-gel; Manganites; Perovskite; Magnetic properties; Rietveld analysis.

## Introduction

Perovskite oxide is generally described by stoichiometric formula  $\text{ABO}_3$ , where A and B represent a lanthanide (or alkaline earth ion) and a transition metal ion, respectively. The structural tolerance factor ( $t$ ) for these oxides ranges from 0.75 to 1, which helps in multiple cation substitutions for cations with small difference in their ionic sizes [1, 2]. Perovskite manganites with the general formula  $\text{R}_{1-x}\text{A}_x\text{MnO}_3$  (where R is a rare earth element and A is a divalent alkaline earth metal) have received much attention in the recent years due to the discovery of the colossal magnetoresistance (CMR) and its potential applications [3–8].

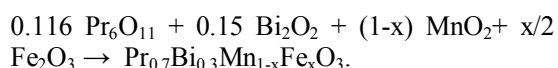
The functional properties of perovskite oxides are generally influenced by the synthesis methods, calcination conditions (temperature, time and atmosphere) and A and / or B site substitution [9–12]. The transport properties of perovskite can be altered by the partial

substitution of A-site cation by other proper cations, e.g. lanthanum by strontium [13, 14] or cerium [15, 16]. However, the catalytic activity of perovskites is mainly controlled by the type of cation type occupying B site and the partial substitution of the site [1, 2, 17–19]. Substitutions in the A and/or B sites create defects and hence modify the catalytic and other functional properties [15, 20]. Many techniques have been employed to elaborate perovskites-based rare-earth manganites; *i.e.*, as conventional solid-state reaction [21], combustion thermal spray [22] and sol-gel [23]. The sol-gel method is an important ceramic oxide technique generally used to prepare nanopowders. It involves several advantages like short reaction time, low reaction temperature, besides producing homogeneous products with high purity.

In the present paper, we report the structural, morphological and magnetic properties of  $\text{Pr}_{0.7}\text{Bi}_{0.3}\text{Mn}_{1-x}\text{Fe}_x\text{O}_3$  with  $x = 0, 0.1$  and  $0.2$  samples elaborated by sol-gel method.

## Experimental

The  $\text{Pr}_{0.7}\text{Bi}_{0.3}\text{Mn}_{1-x}\text{Fe}_x\text{O}_3$  samples were prepared by a modified sol-gel method [24-26] by mixing  $\text{Pr}_6\text{O}_{11}$ ,  $\text{MnO}_2$ ,  $\text{Bi}_2\text{O}_3$  and  $\text{Fe}_2\text{O}_3$  up to 99.9 % purity in stoichiometric proportions used in the desired proportion, according to the following reaction:



The starting materials  $\text{Pr}_6\text{O}_{11}$ ,  $\text{MnO}_2$ ,  $\text{Bi}_2\text{O}_3$  and  $\text{Fe}_2\text{O}_3$  were dissolved in dilute nitric acid at  $90^\circ\text{C}$  and then suitable amounts of citric acid and ethylene glycol as coordinate agents were added. The resulting gel was decomposed at  $300^\circ\text{C}$  and the acquired precursor powder was heated in air at  $1000^\circ\text{C}$  for 3 hours to improve the structure and homogeneity.

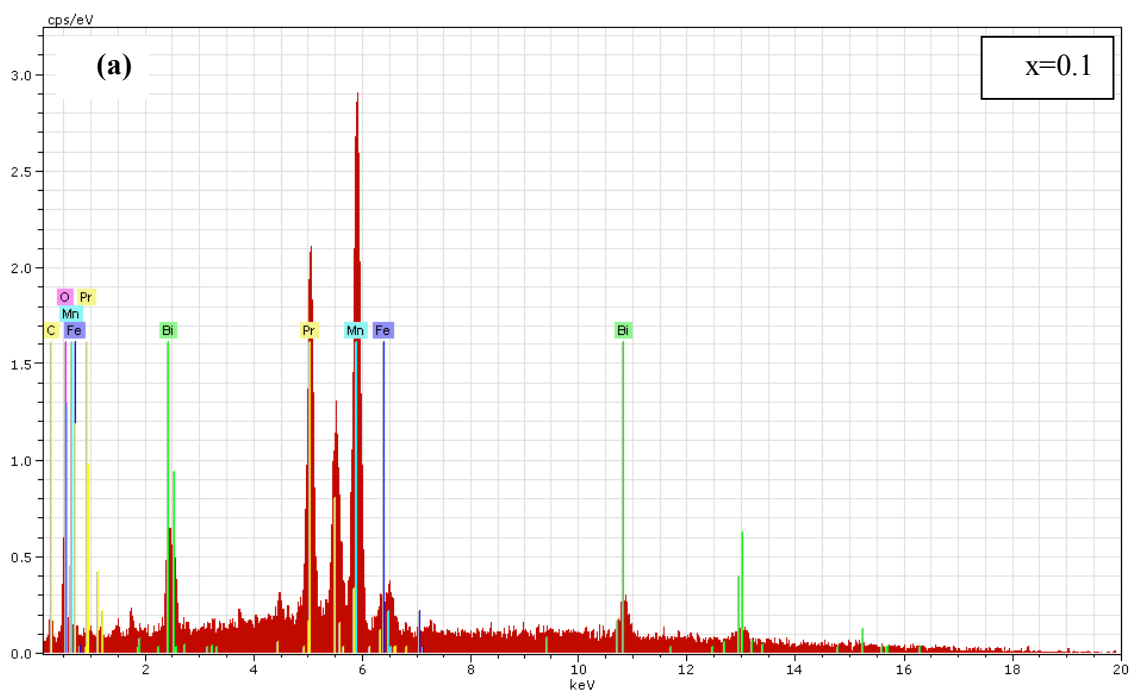
Phase purity, homogeneity and crystal properties were determined by powder X-ray diffraction at room temperature using a

SIEMENS D500 diffractometer with  $\text{CuK}_\alpha$  radiation source in the range from  $20^\circ$  to  $80^\circ$  by the Rietveld analysis. The average particle size of the samples was estimated from X-ray peak width by using the Scherrer formula, and also from the SEM micrograph. Furthermore, the structural analysis of the compound has been carried out using Fourier transform infrared spectroscopy (FTIR) spectroscopic technique. The magnetization measurements were carried out using a vibrating sample magnetometer in the temperature range 2–150 K under an applied field up to 0.05 T.

## Results and Discussion

### Energy Dispersive Analysis of X-ray (EDAX)

In order to check the existence of all elements in our powders, an example of the energy dispersive analysis of X-ray analysis (EDAX) of  $\text{Pr}_{0.7}\text{Bi}_{0.3}\text{Mn}_{1-x}\text{Fe}_x\text{O}_3$  ( $x = 0.1$  and  $x = 0.2$ ) was performed in Figs. 1(a) and (b). The EDAX spectra revealed the presence of oxygen (O), bismuth (Bi), praseodymium (Pr) and manganese (Mn) in appropriate concentrations, confirming that there is no loss of any integrated element during the sintering.



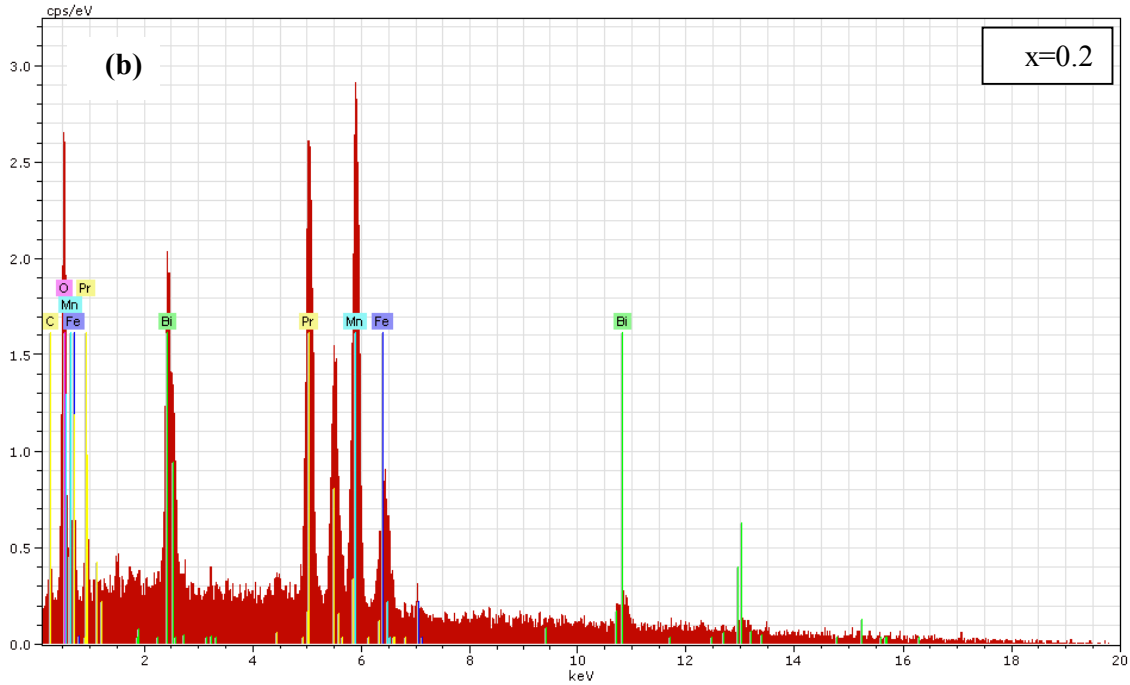
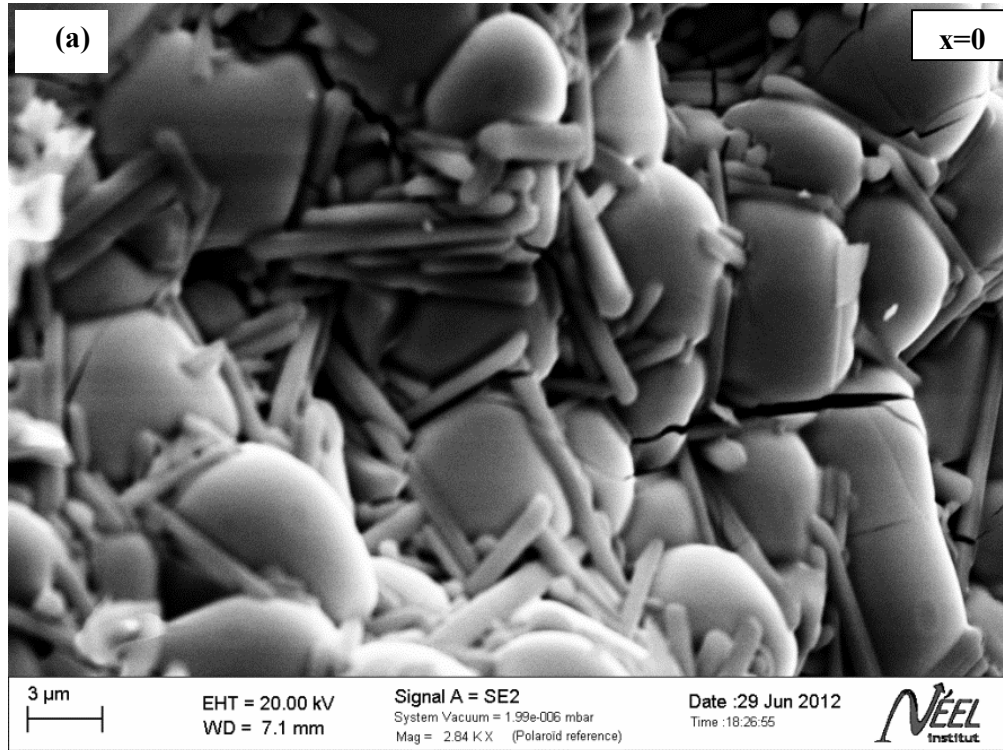


FIG. 1. EDAX analysis of  $\text{Pr}_{0.7}\text{Bi}_{0.3}\text{Fe}_x\text{Mn}_{1-x}\text{O}_3$  (a:  $x=0.1$  and b:  $x=0.2$ ) compounds.

### Scanning Electron Microscopy

Scanning Electron Microscopy was used to check the morphology and particle size as seen in Figs. 2(a) - (c). The nature, shape and distribution of grains suggest that all compounds have polycrystalline characteristics. Some

agglomerations are shown on each pellet surface. The major morphology of these samples was huge gray grains with grain sizes in the range of a few micrometers. In addition, we can clearly observe that the grain size is different in all the samples.



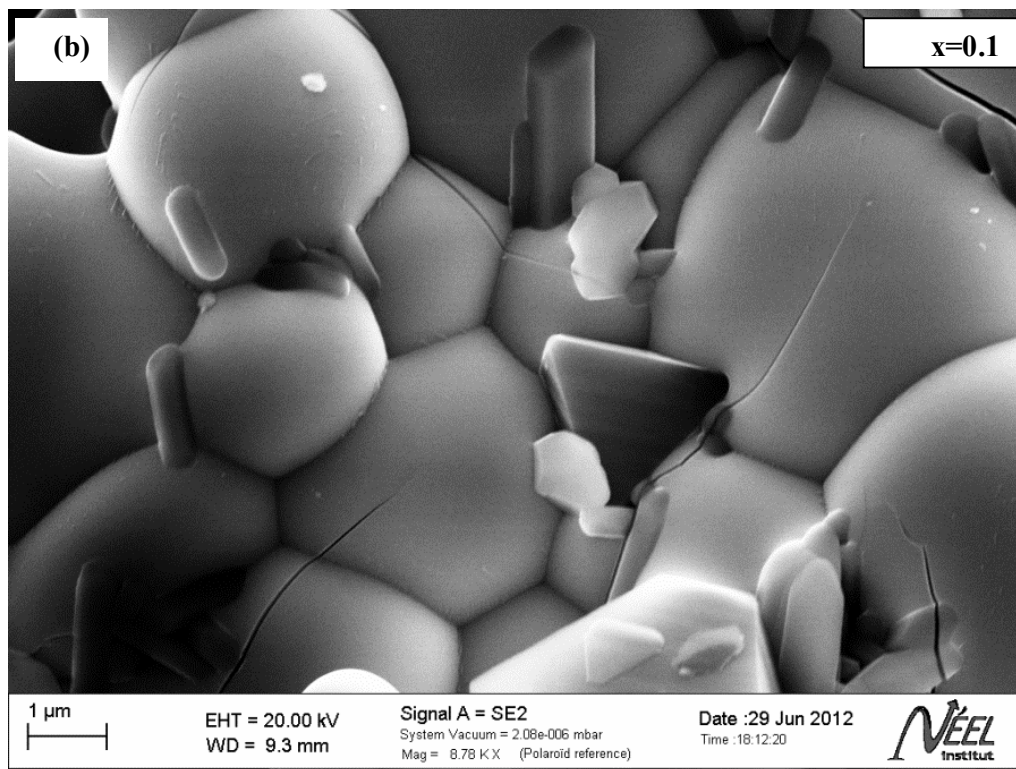
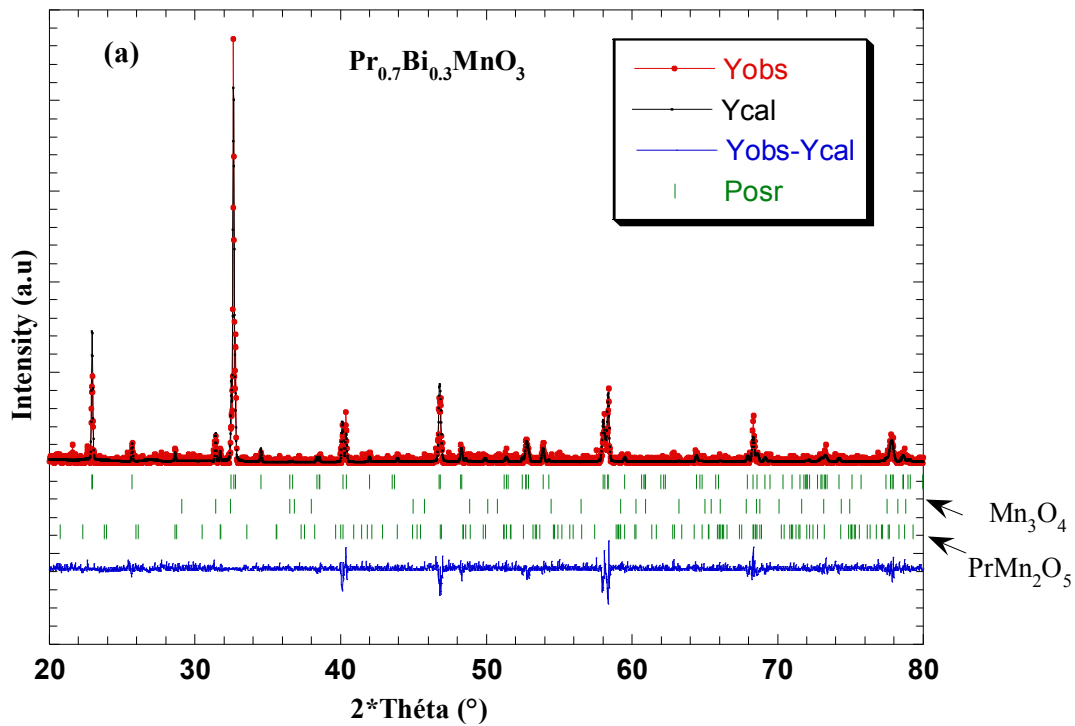


FIG. 2. SEM micrographs of  $\text{Pr}_{0.7}\text{Bi}_{0.3}\text{Fe}_x\text{Mn}_{1-x}\text{O}_3$  (a:  $x = 0$ , b:  $x=0.1$  and c: 0.2) compounds.

### Structural Properties

The powder X-ray diffraction (XRD) was used to verify the crystal structure of the samples. The XRD pattern and the Rietveld analysis using the FULLPROF program [27, 28] are shown in Figs. 3 (a) - (c). For all samples, the X-ray data are fitted to three different phases; the first one corresponding to  $\text{Pr}_{0.7}\text{Bi}_{0.3}\text{Mn}_{1-x}\text{Fe}_x\text{O}_3$  fitted in the orthorhombic structure with the  $\text{Pnma}$  space group, the second phase corresponding to unreacted  $\text{Mn}_3\text{O}_4$ , space group **I 41/amd** and the third one corresponding to  $\text{PrMn}_2\text{O}_5$  in the orthorhombic structure with the **Pbam** space group. The red continuous line indicates the experimental data, and the calculated data is the continuous black line

overlapping them. The lowest curve shows the difference between experimental and calculated patterns. The vertical bars indicate the expected reflection positions. The unit cell volume and the lattice parameters obtained by whole pattern refinements are given in Table 1. The quality of the refinement is evaluated through several parameters such as the pattern R factor ( $R_p$ ) and the goodness-of-fit indicator ( $\chi^2$ ). We note that Pr/Bi atoms have been located at 4c ( $x, 0.25, z$ ) position, Mn/Fe atoms at 4b ( $0, 0, 0.5$ ) and oxygen atoms occupy two different sites; namely  $\text{O}_1$  at 4c ( $x, 0.25, z$ ) and  $\text{O}_2$  at 8d ( $x, y, z$ ) positions. The structural refinement data are reported in Table 2.



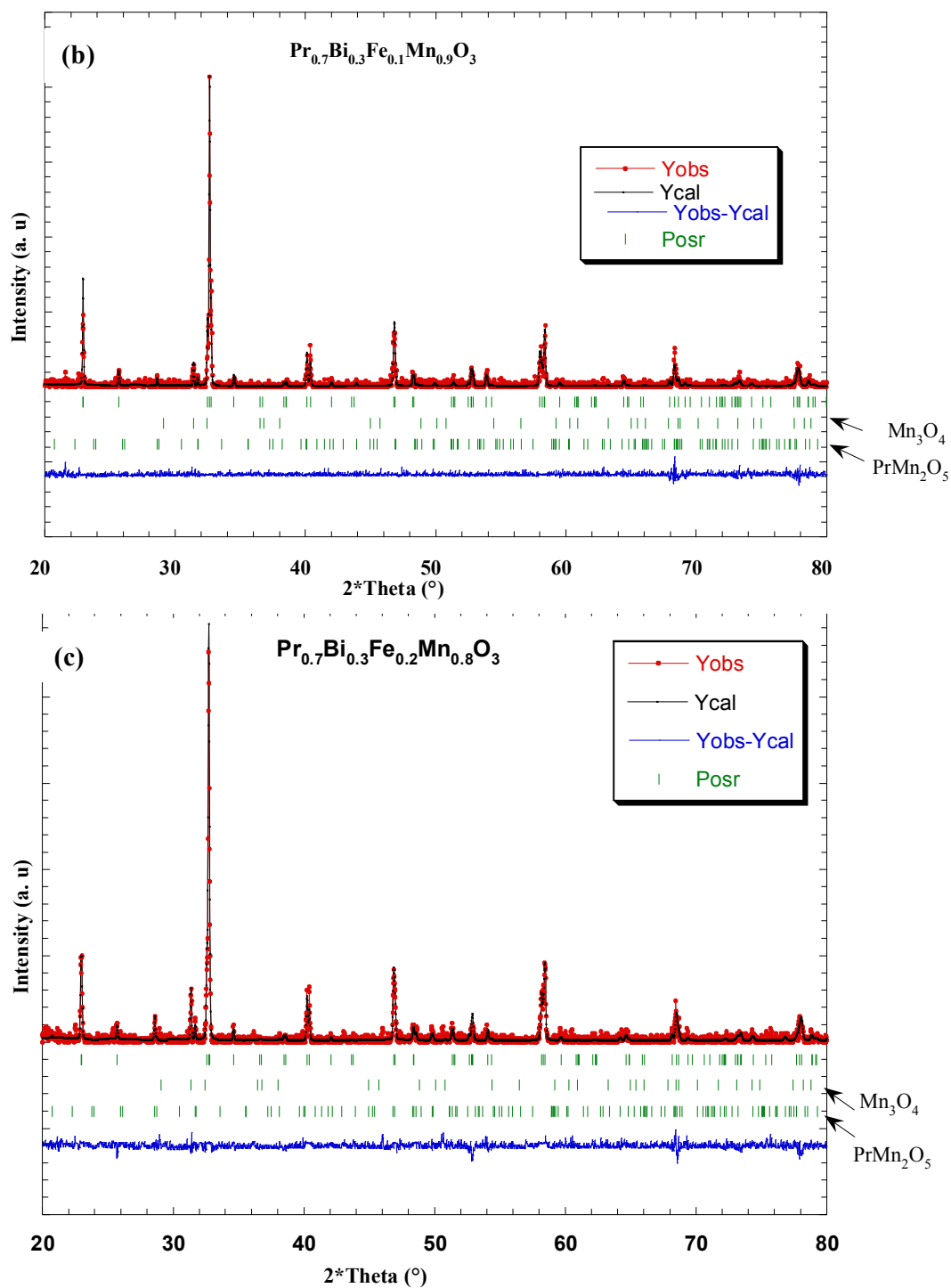


FIG. 3. Powder X-ray diffraction pattern and refinement of  $\text{Pr}_{0.7}\text{Bi}_{0.3}\text{Fe}_x\text{Mn}_{1-x}\text{O}_3$  (a:  $x = 0$ , b:  $x = 0.1$  and c:  $x = 0.2$ ) compounds.

TABLE 1. Unit cell parameters and volume of  $\text{Pr}_{0.7}\text{Bi}_{0.3}\text{Fe}_x\text{Mn}_{1-x}\text{O}_3$  ( $x = 0, 0.1$  and  $0.2$ ).

Samples	a (Å)	b (Å)	c (Å)	V (Å <sup>3</sup> )
x = 0	5.513 <sub>5</sub>	7.7581 <sub>6</sub>	5.4718 <sub>2</sub>	234.05
x = 0.1	5.504 <sub>9</sub>	7.739 <sub>4</sub>	5.4695 <sub>2</sub>	233.05
x = 0.2	5.492 <sub>1</sub>	7.733 <sub>1</sub>	5.4626 <sub>6</sub>	232.01

TABLE 2. Refined structural parameter  $\text{Pr}_{0.7}\text{Bi}_{0.3}\text{Fe}_x\text{Mn}_{1-x}\text{O}_3$  ( $x = 0, 0.1$  and  $0.2$ ) samples. Numbers in subscript represent the error bars.

Samples	x = 0	x = 0.1	x = 0.2
<b>Pr/Bi</b>			
x	0.0326 <sub>6</sub>	0.0289 <sub>5</sub>	0.0201 <sub>6</sub>
y	0.25	0.25	0.25
z	0.0115 <sub>9</sub>	0.0115 <sub>9</sub>	0.0116
x	0.0326 <sub>6</sub>	0.0289 <sub>5</sub>	0.0201 <sub>6</sub>
<b>Mn/Fe</b>			
x	0	0	0
y	0	0	0
z	0.5	0.5	0.5
<b>O1</b>			
x	0.4927 <sub>4</sub>	0.4926 <sub>5</sub>	0.4927 <sub>5</sub>
y	0.25	0.25	0.25
z	0.2208 <sub>1</sub>	0.2206 <sub>1</sub>	0.2206 <sub>9</sub>
<b>O2</b>			
x	0.2842 <sub>8</sub>	0.2785 <sub>4</sub>	0.2936 <sub>1</sub>
y	0.0040	0.0070 <sub>8</sub>	0.0242
z	0.7527 <sub>8</sub>	0.6883 <sub>3</sub>	0.6995 <sub>2</sub>
$\chi^2$	1.06	1.04	1.16
$R_f$	15.7	19.3	34.3

Our crystallographic parameters were found to be similar to those obtained by Rudskaya et al. [29] for  $\text{Pr}_{0.7}\text{Bi}_{0.3}\text{MnO}_3$  sample elaborated by solid state reaction. They are also similar to those obtained by Chand et al. [30] for  $\text{Pr}_{0.7}\text{Sr}_{0.3}\text{MnO}_3$  powder synthesized by Sol-gel method, and to those obtained by Cherif et al. [31] for  $\text{Pr}_{0.67}\text{Sr}_{0.33}\text{MnO}_3$  manganite oxide prepared by ball milling method.

The Mn atom is coordinated by six oxygen atoms forming octahedral, almost regular. Fig. 4 shows the crystal structure of  $\text{Pr}_{0.7}\text{Bi}_{0.3}\text{MnO}_3$  and the coordination polyhedron on Mn, and the distances between Mn and the first neighbor oxygen are so that there are three different Mn–O distances. The interatomic distances for the  $\text{Pr}_{0.7}\text{Bi}_{0.3}\text{Mn}_{1-x}\text{Fe}_x\text{O}_3$  (with  $x = 0, 0.1$  and  $0.2$ ) samples are listed in Table 3.

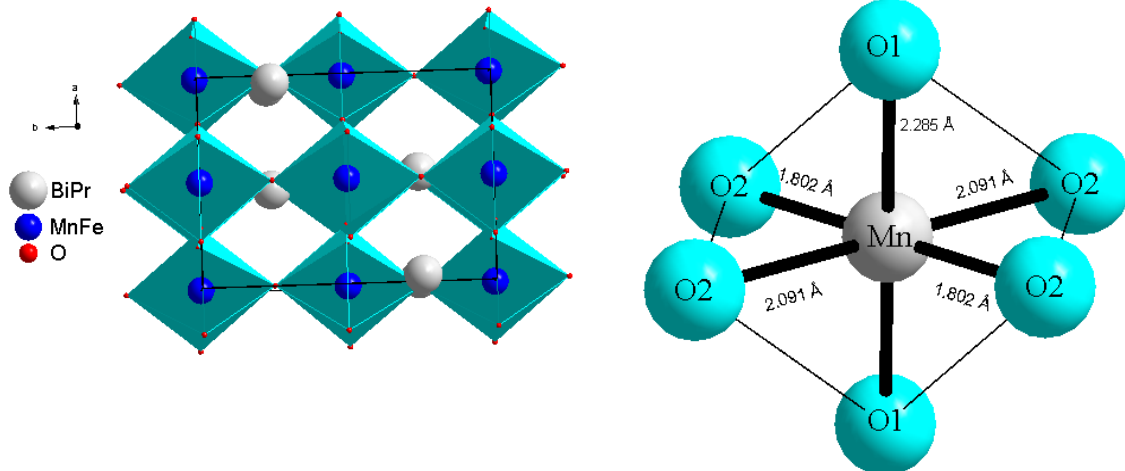
FIG. 4. Crystal structure of  $\text{Pr}_{0.7}\text{Bi}_{0.3}\text{MnO}_3$  and the coordination polyhedron on Mn.

TABLE 3. The interatomic distances for the  $\text{Pr}_{0.7}\text{Bi}_{0.3}\text{Fe}_x\text{Mn}_{1-x}\text{O}_3$  ( $x = 0, x=0.1$  and  $0.2$ ) samples.

Samples	x=0	x=0.1	x=0.2
<b>Distances (Å)</b>			
Mn–O(1)	2.09	2.28	2.27
Mn–O(2)	2.22	2.24	2.00
Mn–O(2)	2.45	2.09	1.95
<b>Angles (°)</b>			
Mn–O(2)–Mn	175.98	175.98	156.11
Mn–O(1)–Mn	112.63	112.63	116.08
O(1)–Mn–O(1)	180	180	180
O(1)–Mn–O(2)	135.20	145.01	144.66
O(2)–Mn–O(2)	180	180	180

The change of average ionic radius  $\langle r_A \rangle$  influences the unit cell volume. The influence can be explained by its ability to modify the Mn–O distances and Mn–O–Mn angles, and consequently the distortion of the ideal perovskite structure in which the Mn–O–Mn angle is equal to  $180^\circ$ . To confirm this, we calculated the Mn–O distances and Mn–O–Mn angles for  $\text{Pr}_{0.7}\text{Bi}_{0.3}\text{MnO}_3$  nanopowders.

To corroborate experimental observation, the result has been compared to the Goldsmid [32] tolerance factor ( $t$ ):

$$t = \frac{r_A + r_O}{\sqrt{2}(r_B + r_O)}$$

with  $r_O = r(\text{O}^{2-}) = 1.32 \text{ \AA}$ ,  $r(\text{Mn}^{3+}) = 0.645 \text{ \AA}$ ,  $r(\text{Mn}^{4+}) = 0.53 \text{ \AA}$ ,  $r(\text{Bi}^{3+}) = 1.52 \text{ \AA}$  and  $r(\text{Pr}^{3+}) = 1.179 \text{ \AA}$ .

The  $r_A$ ,  $r_B$  and  $r_O$  are the ionic radii of A, B and O site atoms in  $\text{ABO}_3$  structure, respectively [33, 34]. In the perovskite type compounds, the tolerance factor is between  $0.78 < t < 1.05$  [35]. It should be noticed that the value equals unity for ideal structure. For our nanopowders, the tolerance factor ( $t$ ) is about 0.80, pointing out that our nanopowders have an orthorhombic perovskite structure. This result is in agreement with the results found by Tomioka and Tokura [36]. The average particle diameter  $D$  for different specimens was obtained from the main peaks of the X-ray powder diffraction using Scherer's formula [37] for the peak width broadening as a function of the size of the particles.

$$D = \frac{k\lambda}{\beta \cos(\theta)} \quad (1)$$

where  $\lambda$  ( $\text{CuK}\alpha = 1.5418 \text{ \AA}$ ), is the X-ray wavelength,  $k$  is the machine constant (0.916),  $\theta$  and  $\beta$  are the diffraction angle and the full width for the most intense peak with.

$$\beta = \beta_m^2 - \beta_i^2 \quad (2)$$

$\beta_m$  is the experimental full width at half maximum (FWHM),  $\beta_i$  is the FWHM of a standard silicon sample and  $\theta$  is the peak position. The obtained  $D$  values are about 60 nm regardless of the compounds. The  $D$  values are found to be 50, 55 and 62 nm for  $x = 0, x=0.1$  and  $x = 0.2$  samples, respectively.

### FTIR Spectroscopy

Among numerous applications of vibrational spectroscopy to solid-state problems, those dealing with structural evolution of samples obtained by sol–gel process appear particularly interesting. IR spectroscopy gives qualitative information about the way in which the adsorbed molecules are bounded to the surface as well as structural information of solids. The spectra of  $\text{Pr}_{0.7}\text{Bi}_{0.3}\text{Mn}_{1-x}\text{Fe}_x\text{O}_3$  nanopowders are given in Fig. 5. The observed band at  $571 \text{ cm}^{-1}$  corresponds to  $\nu(\text{MnO}_2)$  stretching mode that involves the internal motion of change in the Mn–O–Mn bond length [38]. The peak observed at  $970 \text{ cm}^{-1}$  is attributed to the deformation and O–H stretching mode of absorbed water molecules [39].

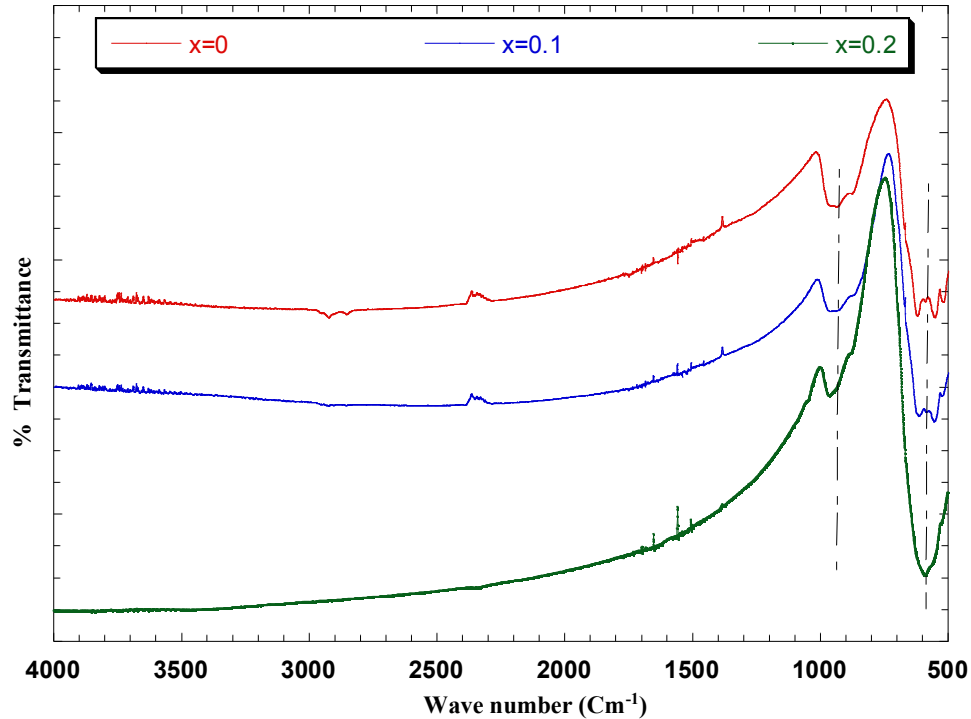


FIG. 5. Fourier transform infrared (FTIR) transmission spectrum of  $\text{Pr}_{0.7}\text{Bi}_{0.3}\text{Fe}_x\text{Mn}_{1-x}\text{O}_3$  ( $x = 0, 0.1$  and  $0.2$ ) compounds at room temperature.

### Magnetic Properties

The temperature dependence of the magnetization  $M$  (T) under an applied magnetic field of 0.05 T for the  $\text{Pr}_{0.7}\text{Bi}_{0.3}\text{Mn}_{1-x}\text{Fe}_x\text{O}_3$  ( $0 \leq x \leq 0.2$ ) samples is shown in Fig. 6. The magnetization decreases with increasing Fe content. All samples show an anti-ferromagnetic paramagnetic AFM-PM transition, at Neel temperature  $T_N$ . The  $T_N$  temperature values were determined from  $dM/dT$  curves. The Neel temperature is found to increase from 42 K for  $x = 0$  to 45 K for  $x = 0.2$  for the  $\text{Pr}_{0.7}\text{Bi}_{0.3}\text{Mn}_{1-x}\text{Fe}_x\text{O}_3$  samples. The magnitude of the magnetization at low temperature decreases with increasing Fe content. The iron doping induces a weakening of the ferromagnetism at low temperatures. This weakening can be explained by the competition between the  $(\text{Mn}^{3+}-\text{O}-\text{Mn}^{4+})$  double exchange and the  $(\text{Fe}^{3+}-\text{O}-\text{Mn}^{4+})$  superexchange.

In order to investigate the magnetic behavior of the system at low temperature, we have carried out magnetization measurements *versus* the magnetic applied field up to 6 T at 5 K, Fig. 7. From this figure, we see that the magnetization decreases with increasing Fe content. In fact, the magnetization is not saturated, this is associated with the relaxations

in the nanoparticles of the samples and also due to the presence of the AFM interactions caused by the important content of iron in the structure.

The values of the saturation magnetization were calculated using the total spins of  $\text{Mn}^{3+}$ ,  $\text{Mn}^{4+}$ ,  $\text{Fe}^{3+}$  and  $\text{Pr}^{3+}$  ions ( $\mu_{\text{Mn}^{3+}} = 4 \mu_B$ ,  $\mu_{\text{Mn}^{4+}} = 3 \mu_B$ ,  $\mu_{\text{Fe}^{3+}} = 5 \mu_B$ , and  $\mu_{\text{Pr}^{3+}} = 2 \mu_B$ ). The saturation magnetization of the  $\text{Pr}_{0.7}^{3+}\text{Bi}_{0.3}^{2+}(\text{Mn}_{1-x}\text{Fe}_x)_{0.7}^{3+}\text{Mn}_{0.3}^{4+}\text{O}_2^{3-}$  compounds is expressed as:

$$M_{\text{sat}} = [4 \times 0.7 \times (1 - x)] - 5 \times (0.7 \times x) + 3 \times 0.3 + 2 \times 0.7] \mu_B = [5.1 - 6.3 \times x] \mu_B$$

where  $x$  is the iron content and  $\mu_B$  is the Bohr magneton. The calculated values of saturation magnetization for full spin alignment of all the magnetic moments for  $(x = 0, 0.1$  and  $0.2)$  are found to be  $5.1 \mu_B$ ,  $4.47 \mu_B$  and  $3.84 \mu_B$ , respectively. The measured values of saturation magnetization at  $T = 5$  K for  $(x = 0, 0.1$  and  $0.2)$  are found to be  $3.17 \mu_B$ ,  $2.01 \mu_B$  and  $1.81 \mu_B$ , respectively. The saturation magnetization decreases with increasing Fe content which confirms that the magnetic moments of the Fe are coupled antiparallel with the Mn one. The difference between measured and calculated values especially should be explained by spin canted state at low temperature as well as the presence of  $\text{Mn}_3\text{O}_4$  as a secondary phase.

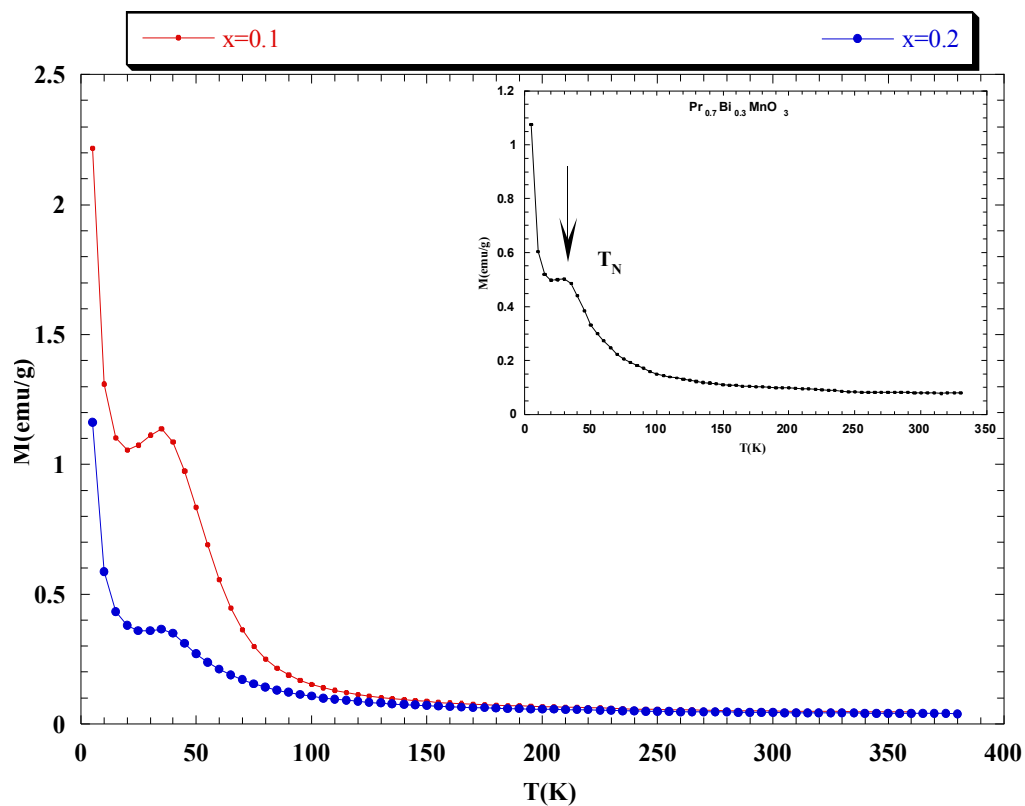


FIG. 6. Temperature dependence of the magnetization of  $\text{Pr}_{0.7}\text{Bi}_{0.3}\text{Fe}_x\text{Mn}_{1-x}\text{O}_3$  ( $x = 0, 0.1$  and  $0.2$ ) at  $H = 0.05$  T.

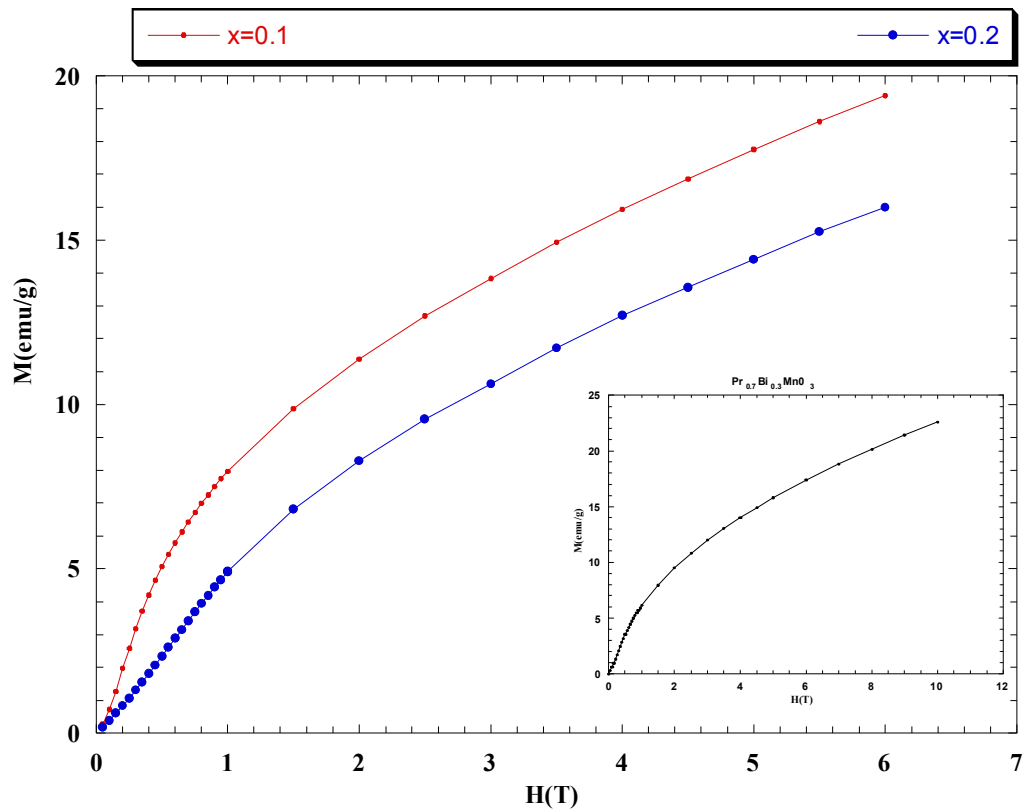


FIG. 7. Variation of magnetization as a function of applied magnetic field measured at 5 K for  $\text{Pr}_{0.7}\text{Bi}_{0.3}\text{Fe}_x\text{Mn}_{1-x}\text{O}_3$  ( $x = 0, 0.1$  and  $0.2$ ).

## Conclusion

$\text{Pr}_{0.7}\text{Bi}_{0.3}\text{Mn}_{1-x}\text{Fe}_x\text{O}_3$  powder samples have been synthesized using the sol-gel method for the composition range  $0 \leq x \leq 0.2$ . We have investigated their structural, morphological and magnetic properties. Our synthesized samples crystallize in the orthorhombic structure with Pnma space group. Using Scherer's formula, all our samples have a grain size less than 65 nm. The FTIR spectra revealed the presence of the stretching and bending modes for all samples. Our synthesis samples exhibit an

antiferromagnetic-paramagnetic transition when temperature increases. The magnetic transition temperature  $T_N$  increases slightly with the presence of iron in the structure, which confirms that the magnetic moments of iron are coupled antiparallel with the Mn one.

## Acknowledgements

This work has been supported by the Tunisian Ministry of Scientific Research and Technology and the Neel Institute.

## References

- [1] Tanaka, H. and Misono, M., *Curr. Opin. Solid State Mater. Sci.*, 5 (2001) 381.
- [2] Yamazoe, N. and Teraoka, Y., *Catal. Today*, 8 (1990) 175.
- [3] Rao, C.N.R. and Raveau, B., "World Scientific", (Singapore, 1998).
- [4] Dhahri, A., Dhahri, J., Zemni, S., Oumezzine, M., Said, M. and Vincent, H., *J. Alloys Compd.*, 450 (2008) 12.
- [5] Dagotto, E., *New J. Phys.*, 7 (2005) 67.
- [6] Pattabirama, M., Adepub, R., Singh, N.P., Venkatesh, R., Angappane, Ramaa, S.N. and Rangarajan, G., *J. Alloys Compd.*, 452 (2008) 230.
- [7] Hua, X.K., Xub, M.H., Wang, Z.S., Wua, Z.S.Y. and Si, Q.P.Z., *Solid State Commun.*, 149 (2009) 243.
- [8] Dhahri, N., Dhahri, A., Cherif, K., Dhahri, J., Belmabrouk, H. and Dhahri, E., *J. Alloys Compd.*, 507 (2010) 405.
- [9] Campagnoli, E., Tavares, A.L., Fabbrini, Rossetti, I., Dubitsky, Y.A., Zaopo, A. and Forni, L., *Appl. Catal. B. Env.*, 55 (2005) 133.
- [10] Liu, S., Tan, X., Li, K. and Hughes, R., *Ceram. Int.*, 28 (2002) 327.
- [11] Leontiou, A., Ladavos, A.K. and Pomonis, P.J., *Appl. Catal. A: Gen.*, 241 (2003) 133.
- [12] Kleveland, K., Einarsrud, M.A. and Grande, T., *J. Eur. Ceram. Soc.*, 20 (2000) 185.
- [13] Klvana, D., Vaillancourt, J., Kirchnerova, J. and Chaouki, J., *Appl. Catal. A. Gen.*, 109 (1994) 181.
- [14] Gunasekaran, N., Saddawi, S. and Carberry, J.J., *J. Catal.*, 159 (1996) 107.
- [15] Alifanti, M., Auer, R., Kirchnerova, J., Thyron, F., Grange, P. and Delmona, B., *Appl. Catal. B: Env.*, 41 (2003) 71.
- [16] Nitadori, T. and Misono, M., *J. Catal.*, 93 (1985) 459.
- [17] Azada, K., Eriksson, S.G., Ivanov, S.A., Mathieu, R., Svedlindh, P., Eriksen, J. and Rundlof, H., *J. Alloys. Compd.*, 364 (2004) 77.
- [18] Buciuman, F.C., Patcas, F., Menezo, J.C., Barbier, J., Hahn, T. and Lintz, H.G., *Appl. Catal. B: Env.*, 35 (2002) 175.
- [19] Spinicci, R., Tofanari, A., Faticanti, M., Pettiti, I. and Porta, P., *J. Mol. Catal. A: Chem.*, 176 (2001) 247.
- [20] Saracco, G., Geobaldo, F. and Baldi, G., *Appl. Catal. B: Env.*, 20 (1999) 277.
- [21] Cherif, K., Zemnia, S., Dhahri, Ja., Dhahri, Je., Oumezzine, M. and Ghedira, H., *J. Alloys Compd.*, 396 (2005) 29.
- [22] Yu, M.H., Devi, S.P., Lewis, L.H., Sampath, S., Parise, J.B. and Gambino, R.J., *Mater. Sci. Eng. B.*, 97 (2003) 245.
- [23] Lin, G.C., Yu, X.L., Wei, Q. and Zhang, J.X., *Mater. Lett.*, 59 (2005) 2149.
- [24] Zayat, H.C. and Levy, M., *D. J. Sol-Gel Sci. Technol.*, 35 (2005) 175.
- [25] Gash, A.E., Tillotson, T.M., Satcher, J.H., Poco, J.F., Urubesh, L.W. and Simpson, R.L., *Chem. Mater.*, 33 (2001) 999.
- [26] Pechini, M.P., U.S. Patent, 3 (1967) 330.

- [27] Rodriguez-Carvajal, J., *Physica B. Condensed Matter*, 192 (1993) 55.
- [28] Rietveld, H.M., *J. Appl. Cryst.*, 2 (1969) 65.
- [29] Rudskaya, A.G., Pustovaya, L.E., Kofanova, N.B. and Kupriyanov, M.F., *Journal of Structural Chemistry*, 47(2006) 711.
- [30] Chand, U., Yadav, K., Gaur, A. and Varma, G.D., *J. of Rare Earths*, 28 (2010) 760.
- [31] Chérif, W., Ellouze, M., Lehlooh, A.-F., Elhalouani, F. and Mahmood, S.H., *J. Magn. Mater.*, 324 (2012) 2030.
- [32] Goldschmidt, V., "Geochemistry", (Oxford University Press, 1958).
- [33] Shannon, R.D., *Gen. Crystallogr.*, 32 (1976) 751.
- [34] Shannon, R.D. and Prewitt, Ch.T., *Sect. B. Cryst. Chem.*, 25 (1969) 925.
- [35] Randall, C.A., Bhalla, A.S., Shrout, T.R. and Cross, L.E., *J. Mater. Res.*, 5 (1990) 829.
- [36] Tokura, Y. and Tomioka, Y., *J. Magn. Mater.*, 200 (1964) 1.
- [37] Guinier, A., X. Dunod (Ed.). (1964) 482.
- [38] Roy, S. and Bandyopadhyay, S., *J. Mater. Sci. Lett.*, 15 (1996) 1872.
- [39] Quijada, M., Cerne, J., Simpson, J.R., Drew, H.D., Ahn, K.H., Millis, A.J., Shreekala, R., Ramesh, R., Rajeswari, M. and Venkatesan, T., *Phys. Rev. B*, 58 (1998) 16093.